INFN - Laboratori Nazionali di Frascati

Servizio Documentazione

LNF-87/16(P)

15 Aprile 1987

A. Aragona, C. Biscari, S. De Simone, E. Gianfelice, S. Guiducci, V. Lollo, S. Pella, M. Preger, M. Serio:

MEASUREMENT AND STEERING OF BEAM POSITION IN ADONE

Expanded Version of paper presented at the
"1987 Particle Accelerator Conference"
March 16-19, 1987 Washington (USA)

Servizio Documentazione
dei Laboratori Nazionali di Frascati
P.O. Box, 13 - 00044 Frascati (Italy)

INFN - Laboratori Nazionali di Frascati
Servizio Documentazione

LNF- 87/16(P)

15 Aprile 1987

MEASUREMENT AND STEERING OF BEAM POSITION IN ADONE

A. Aragona, C. Biscari, S. De Simone, E. Gianfelice*, S. Guiducci, V. Lollo, S. Pella, M. Preger, M. Serio

INFN - Laboratori Nazionali di Frascati, C.P. 13, 00044 Frascati (Roma)
* INFN - Sezione di Napoli, Mostra d'Oltremare, Pad.20, 80125 Napoli

ABSTRACT

The Adone storage ring has been recently equipped with a new beam position detection system consisting of 21 electrostatic pick-up monitors. Absolute accuracy is <0.2 mm with respect to the center of the nearby quadrupoles. Reproducibility is within 0.025 mm. The beam position measurements are used to correct the closed orbit distortion by a least squares minimization, to measure betatron tunes and to perform beam steering for the experimental beam lines.

1 - INTRODUCTION

Adone is a first generation (construction started 1964) e^+/e^- 1.5 GeV storage ring with lattice periodicity 12; focusing in both planes is performed by quadrupole doublets at the ends of bending magnets.

The orbit length is 105 m. The RF harmonic number h is 18, corresponding to 51.411 MHz.

The injection system allows for operation with any number of bunches from 1 to 18. Bunch length is dominated under most operating conditions by anomalous lengthening with values ranging from 20 to 60 cm (4σ). Typical transverse dimensions are 6 mm horizontal and < 2 mm vertical (4σ). Total average current during experimental runs ranges between 30 and 100 mA.

During machine commissioning beam position measurements were performed by means of movable scrapers. The large vacuum chamber aperture and the requirements of high energy physics two beam operation did not call for fast and precise beam position measurements: present operation with a single electron beam is much more demanding from the point of view of beam position measurement, beam steering and orbit correction to ensure the simultaneous operation of different experiments (synchrotron radiation, monochromatic γ-ray beam from backscattering of laser light, free electron laser). For this reason a system of non-destructive electrostatic pick-up stations has been installed during a machine shut-down in the summer of 1986.

2 - MONITOR DESCRIPTION AND CALIBRATION

The only suitable location to install Beam Position Monitors (BPM's) was in the center of the quadrupole doublets. The available space between the quadrupoles is ≈15 cm, preventing the use of flanged units; furthermore in the same region a vacuum pump port must be accomodated.These constraints led to the design depicted schematically in Fig. 1: the BPM is integral part of the quadrupole vacuum chamber, which in turn is referenced to the magnet axis by means of supporting arms. Compensation bellows (not shown in figure) are provided at both ends of the chamber.

Fig. 2 shows a transverse section of the monitor along with the positioning arms in the quadrupole.The BPM is the usual 4-buttons electrostatic monitor type with circular electrodes of radius r = 15 mm mounted flush with the vacuum chamber. The chamber shape is approximately rectangular (total width 2a = 195 mm, total height 2b = 72 mm). The electrode centers are symmetrically located at the corners of a square of side 2b. The BPM center coincides with the quadrupole axis within ± 0.2 mm.

A relativistic bunch induces on the wall of the surrounding vacuum chamber an image current reproducing the longitudinal charge distribution of the bunch. The transverse distribution of such current on the wall depends on beam position and pipe geometry.

Under the assumption of a relativistic bunch much longer than the button, the voltage induced at the i-th electrode is (see Fig. 2).

$$V_i = \frac{2\, i(t)}{c\, a\, C} \int_{x_i-r}^{x_i+r} f_i(x,x_o,y_o)\, \left[r^2 - (x - x_i)^2\right]^{1/2} dx \qquad (1)$$

where i(t) is the instantaneous bunch current; x_o, y_o the beam transverse position, c the speed of

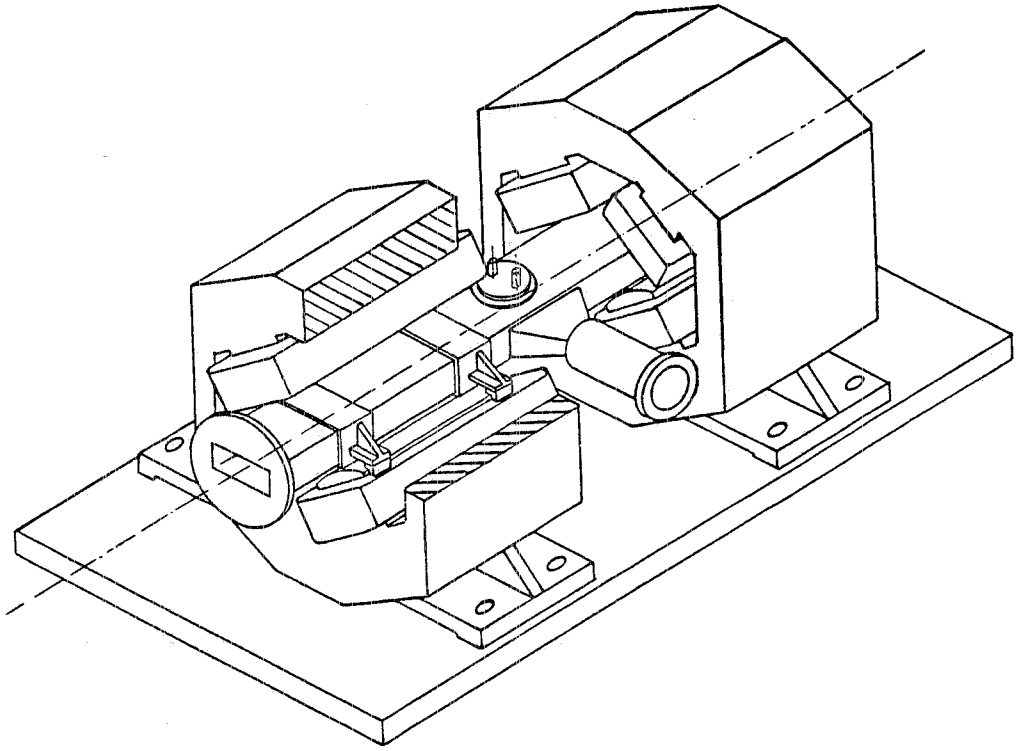

FIG. 1 - View of the BPM assembly.

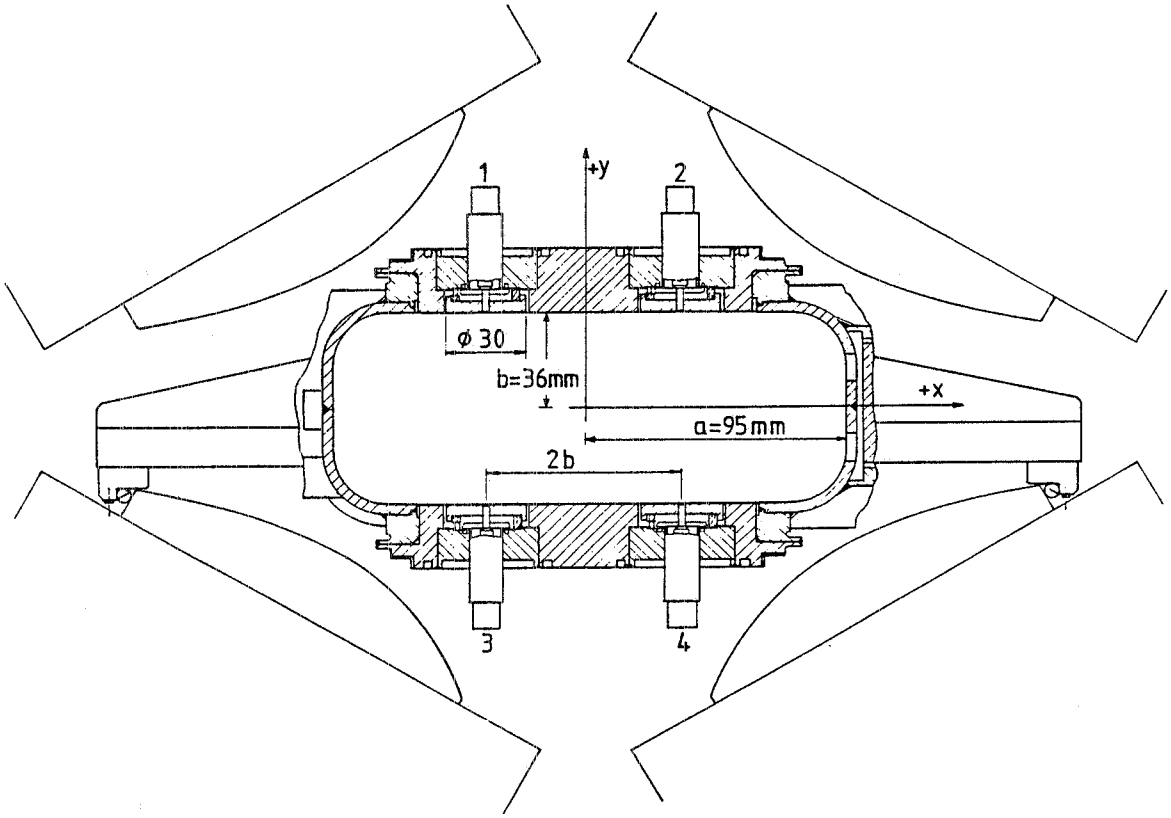

FIG. 2 - Transverse section of a BPM.

light, C the button capacitance to ground, and x_i the button center position; the function f_i is given by (Ref.1)

$$f_i(x,x_o,y_o) = \sum_1^\infty{}_m \frac{\sin[\alpha_m (x_o+a)] \sin[\alpha_m(x+a)] \sinh[\alpha_m(b-s_i y_o)]}{\sinh(2\alpha_m b)} \qquad (2)$$

with $s_i = -1$ for $i = 1,2$ and $s_i = 1$ for $i = 3,4$ and $\alpha_m = m\pi/2a$. By measuring the induced voltages one can in principle deduce the beam position (x_o,y_o).

Before the installation on Adone all monitors have been calibrated in a computer-controlled bench. The TEM field generated in the coaxial system of a wire inside the vacuum chamber simulates the beam electric field. A 0.2 mm diameter wire carrying fast current pulses is stretched in the monitor vacuum chamber by means of a bow support driven by a two-axes positioning stage. The vacuum chamber is supported by reference blocks simulating the quadrupole pole-tip geometry.

The standard calibration procedure consists of two measurement sets: first a small area of 3x3 mm^2 is scanned at 0.5 mm steps to precisely determine the monitor electrical center and to detect possible asymmetries. The center offset is recorded and subtracted from the closed orbit measurements.

The second set of measurements is a scan of a larger area (40 mm horizontal by 30 mm vertical at 2.5 mm steps, and 60 mm horizontal by 50 mm vertical at 5 mm steps) to provide the measured voltages for the calibration. The measurements are in excellent agreement with those numerically evaluated from (1) and (2).

Expressions (1) and (2) are very non-linear in beam position and not suited for inversion with respect to (x_o,y_o). We use therefore an approximate method to deduce the position from the electrode voltages, based on the skew difference method (Ref.2) applied with a recursive linearizing algorithm. We write:

$$U = [(V_2-V_3)/(V_2+V_3) - (V_1-V_4)/(V_1+V_4)]/2 \qquad (3)$$
$$V = [(V_2-V_3)/(V_2+V_3) + (V_1-V_4)/(V_1+V_4)]/2$$

$$x_o = k_x(x_o,y_o)\, U - x_{os} \qquad (4)$$
$$y_o = k_y(x_o,y_o)\, V - y_{os}$$

where (x_{os},y_{os}) is the monitor offset. k_x and k_y have the dimensions of a length and are fitted with the calibration data by a second order polinomial in x_o,y_o. The implicit equations (4) are solved by a recursive method. The process is stopped when two successivly calculated positions coincide within a convergence radius of 0.05 mm.

Fig. 3 shows a nomograph of measured U and V, as defined in (3). Horizontal lines are drawn at constant y_o and vertical ones at constant x_o. The distance between lines is 2.5 mm in the

inner grid and 5 mm in the outer one. Fig. 4 shows the result of the recursive algorithm: lines should be ideally separated by 2.5 mm and 5 mm in the inner grid and in the outer one respectively.

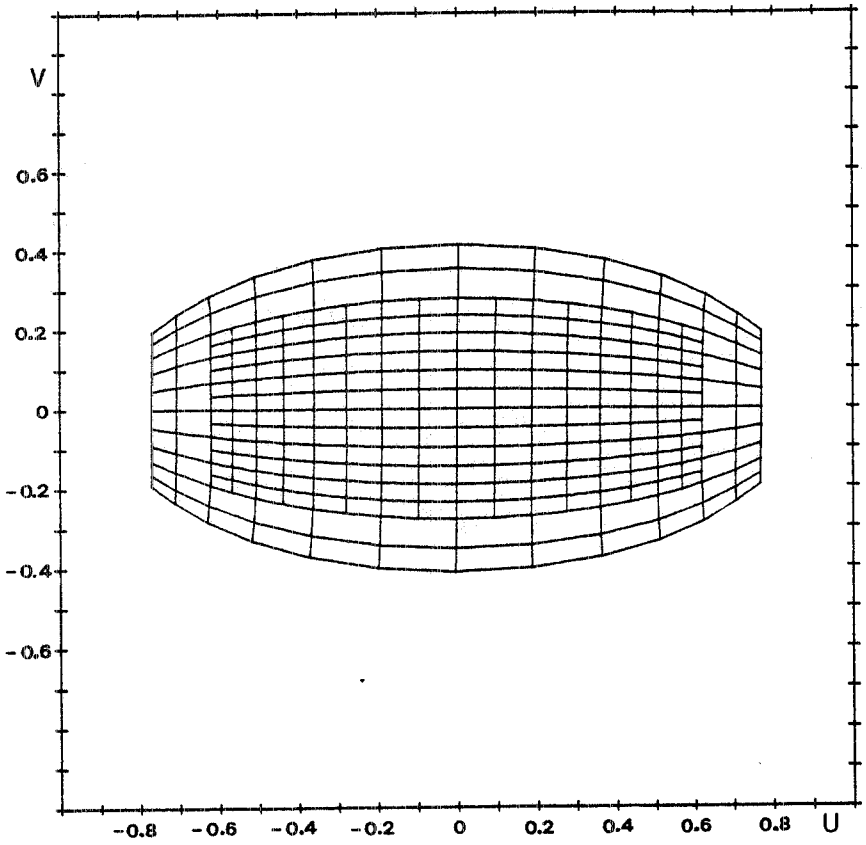

FIG. 3 - Nomograph of measured U and V as defined in (3). Horizontal lines are drawn at constant y_0 and vertical ones at constant x_0. Distance between lines is 2.5 mm for the inner grid, 5.0 mm for the outer.

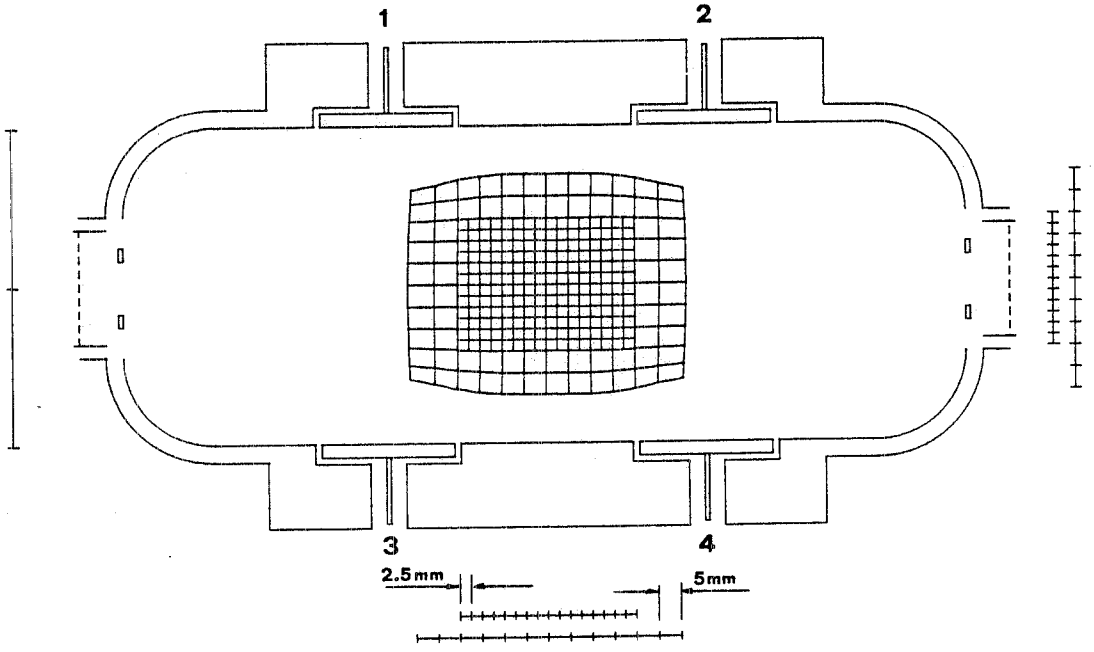

FIG. 4 - Result of the position reconstruction algorithm. Lines should ideally lie 2.5 mm apart from each other in the inner grid, 5 mm in the outer.

3 - MEASUREMENT SYSTEM AND DATA ACQUISITION

The voltage induced by a centered beam in an unloaded electrode is

$$V_0(t) = F\, i(t)\, r^2/(2\, b\, c\, C) \tag{5}$$

where F is an adimensional form factor which depends on the monitor geometry (F is unity in a circular monitor of radius b; in our case F≈0.62), i(t) is the instantaneous bunch current, c the speed of light, and C≈16 pF. By measuring the electrode voltage on the termination resistance of a lossless transmission line with characteristic impedance R_0, the module of the transfer impedance $Z_c(\omega)$ (signal voltage/bunch current) is

$$|Z_c(\omega)| = R_0 \frac{\omega/\omega_1}{[1+(\omega/\omega_2)^2]^{1/2}} \tag{6}$$

ω is the angular frequency and

$$\omega_1 = 2\, b\, c / F\, r^2 \approx 1.6\times10^{11} \text{ rad/s} \tag{7}$$
$$\omega_2 \approx 1 / R_0\, C_e \approx 1.3\times10^{9} \text{ rad/s}$$

In any operating condition of the storage ring the bunch current frequency spectrum has always a component at the 18th harmonic of the revolution frequency .We use a narrow-band system tuned to that frequency to measure the voltages. At this frequency we are in the regime $\omega \ll \omega_2$ where C has little effect on $Z(\omega)$ allowing for some tolerance on the electrode capacitance, and the amplitude of the sinusoidal signal is ≈200 μV/<mA> regardless of the number of bunches, depending only on the total current and, to some extent, on bunch length.

Fig. 5 shows a schematic block diagram of the acquisition system. The sinusoidal component of the electrode signal is narrow-band amplified by a tuned amplification chain (Ref.3). Custom-made narrow-band quartz filters are used to filter out noise. The equivalent input noise is <≈0.2μV rms yielding a good S/N ratio even at very low beam current. The reproducibility in position measurement is of the order of 3μ rms in the calibration bench and ≈25μ horizontal and ≈10μ vertical with the actual beam.

The input and output dynamic range of the amplifiers allows for any possible voltage variation due to beam position, current and number of bunches.

The sinusoidal voltage output is measured by a 4+1/2 digit micro-processor controlled RF voltmeter. The step attenuators are set by the storage ring control computer to yield an average voltage of ≈100 mV at the measuring head in order to exploit the full voltmeter range.

The buttons are sequentially connected to the measuring detector by means of an RF distributed multiplexer (-3 dB BW ≈ 300 MHz) (Ref.4). The multiplexer is composed of a double

shield coaxial cable constituting the Analogic Bus and of "stations" sitting near the quadrupoles. Every station is composed of a SPDT , an SP6T coaxial relay and a digital control board. The function of the first relay is to connect the station to the coaxial cable or to insulate it from the rest of the distributed multiplexer when another station has to be connected. The SP6T relay is used to select one of the BPM electrode buttons or a test signal to check the station functionality. It is possible to connect a terminating resistor to set a zero reference and to check the ohmic continuity. The use of double commutation gives an insulation better than 120 dB (station disconnected); insertion loss is ≈ 1 dB. In the idle position the station is disconnected and the buttons are terminated into 50 Ω load resistors integral to the relay box. The arrow in Fig. 5 indicates the selected button.

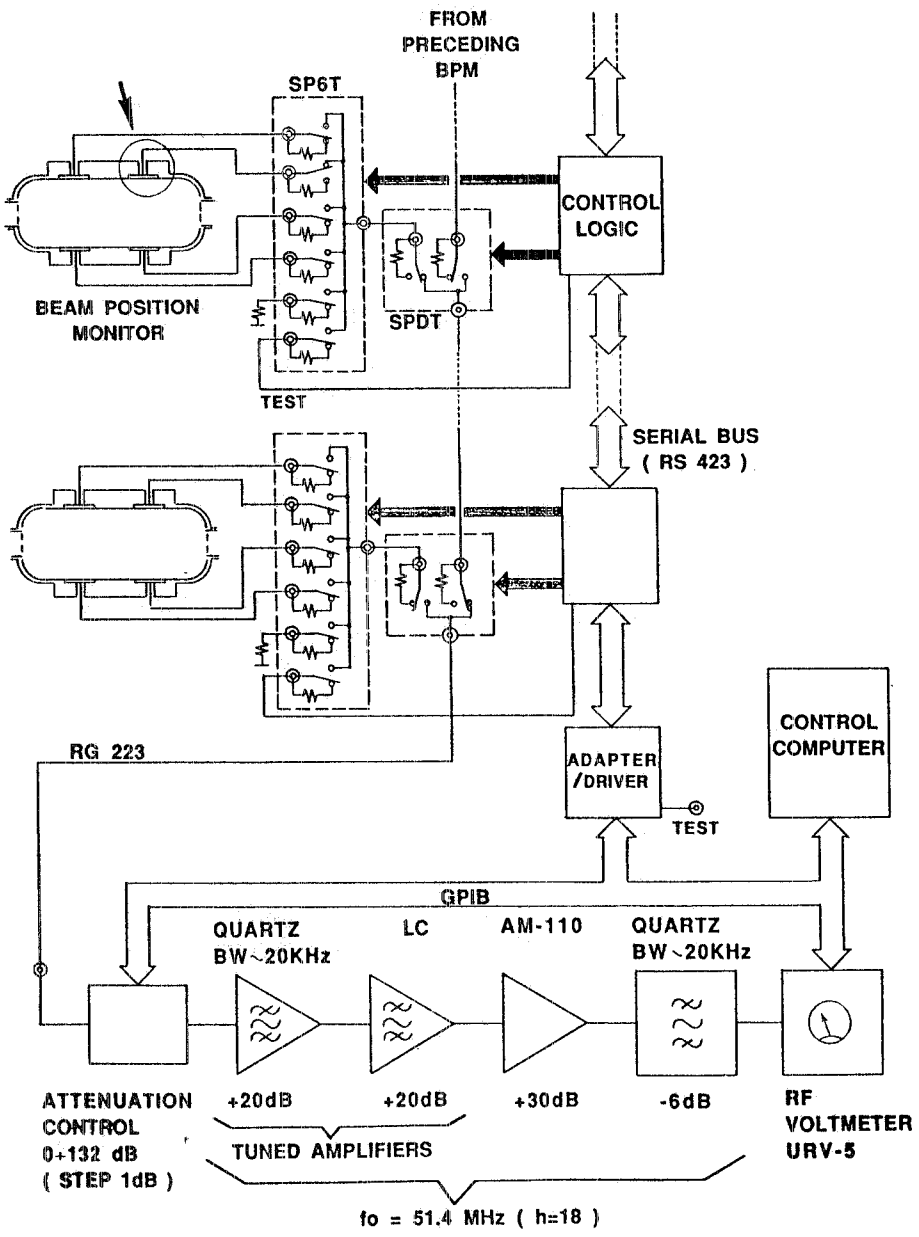

FIG. 5 - Block diagram of the measurement system.

In order to minimize the number of cables, a serial transmission system has been specified for the control boards. The control boards are series-connected in a digital In/Out Bus. Communication takes the form of ASCII command messages preceded by an address. Every station is assigned an address by means of DIP switches uniquely identifying the BPM station number. When the address is recognized commands are executed, otherwise no action is taken and the messages are transmitted back to the next station.

BPM's can be addressed separately or sequentially by the storage ring control computer to measure beam position at selected points or in the whole machine. Closed orbit data are obtained by measured electrode voltages according to the reconstruction algorithm outlined above. Data are checked for consistency and, should the case occur, an alert message indicating poor S/N ratio or possible relay malfunction appears on the operator console. The result of the beam position measurement is displayed on a color TV-screen in the form of a hystogram with vertical lines proportional to the beam displacement at the azimuthal position of each monitor in the ring. Orbit data are stored in a disk file for subsequent analysis, orbit correction and beam steering.

4 - ORBIT CORRECTION LAYOUT

Fig. 6 shows one of the 12 lattice cells. The BPM's are located in the center of the quadrupole doublets, where the two ß functions have approximately the same value. Because of interference with experimental beam lines, 3 out of 24 available positions have not been used.

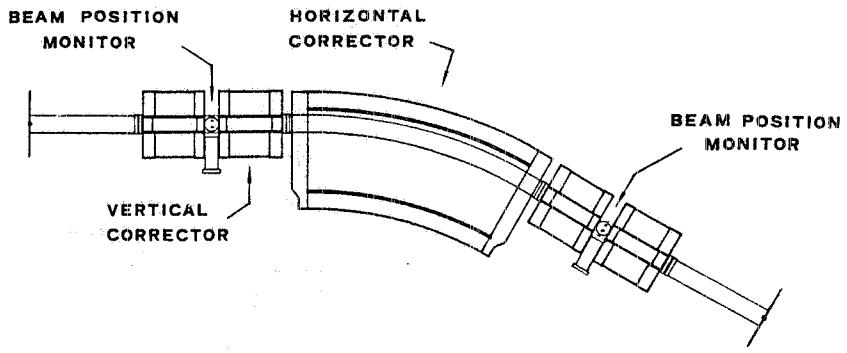

FIG. 6 - The storage ring lattice cell: the center of the straight section and of the bending magnet are symmetry points. The horizontal correctors are backleg windings on the bending magnet, while the vertical ones are realized with dipole windings on one of the two vertically focusing quadrupoles of the cell.

The straight sections are not suited for the installation of correctors, because space must be saved for experimental and machine equipment. Dipole windings in the quadrupoles introduce high-order terms in the magnetic field. In the case of the Adone quadrupoles this effect is tolerable in the vertical plane, but not in the horizontal one. The horizontal correctors are therefore realized with backleg windings on the bending magnets. The major drawbacks of this choice are the poor efficiency of the correction (the horizontal β function has a minimum in the bending magnet) and

the hysteresis effects which show up when the excitation of a large magnet is changed without going through saturation (Ref.5). A typical "hysteresis cycle" induced by the correction winding is shown in Fig. 7, where the measured magnetic field is plotted versus the excitation current in the correction winding (the initial point indicated with A corresponds to the field in the bending magnet before any excitation of the corrector). The reproducibility of the field is compatible with orbit correction requirements after 2-3 complete cycles of the corrector current.

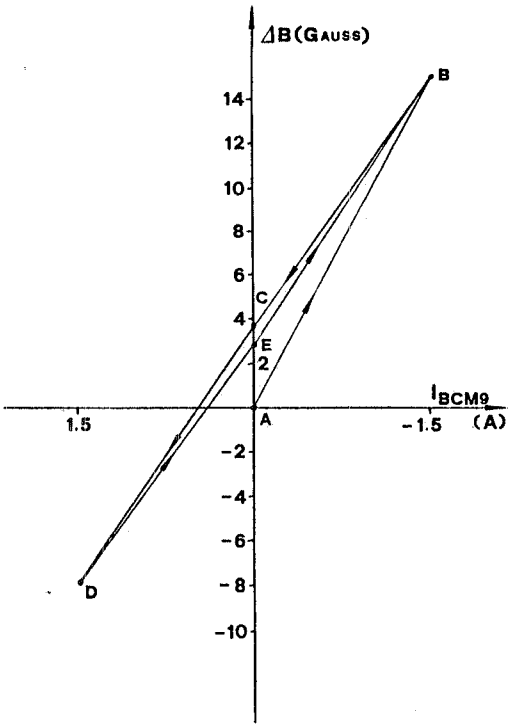

FIG. 7 - Correction field as a function of excitation current in the backleg winding of a bending magnet. Negative current in the corrector increases the field in the magnet and creates a local displacement of the beam towards the center of the ring.

Vertical orbit correction is performed with additional dipole windings in 12 D quadrupoles, where the vertical β approaches its maximum value. The corrector positions are separated by the periodicity of the ring: only one does not follow this rule, because of interference with an experimental beam line. No hysteresis effect induced by vertical correctors has been observed in the quadrupoles.

Fig. 8 shows a schematic layout of the storage ring with all correctors and BPM's: vertical correctors are indicated with the symbol BCQ ("Bobine di Correzione nei Quadrupoli") followed by the number of the corresponding quadrupole. Horizontal ones are denoted by BCM ("Bobine di Correzione nei Magneti") with the number of the corresponding bending magnet. Beam position monitors are indicated by the symbol MP ("Monitor di Posizione") followed by the number of the quadrupole doublet where the monitor is installed (Ref.6).

The typical working point of the machine is near a betatron wavenumber of 3 in both planes: 4 correctors per betatron wavelength are therefore available for orbit correction. A second configuration is also used, with a 6-fold periodicity for the free-electron laser experiment ("LELA", see Ref.7), with vanishing dispersion in 6 straight sections. The horizontal tune of this optics is $\approx$5.15, while the vertical is the same as the normal lattice one.

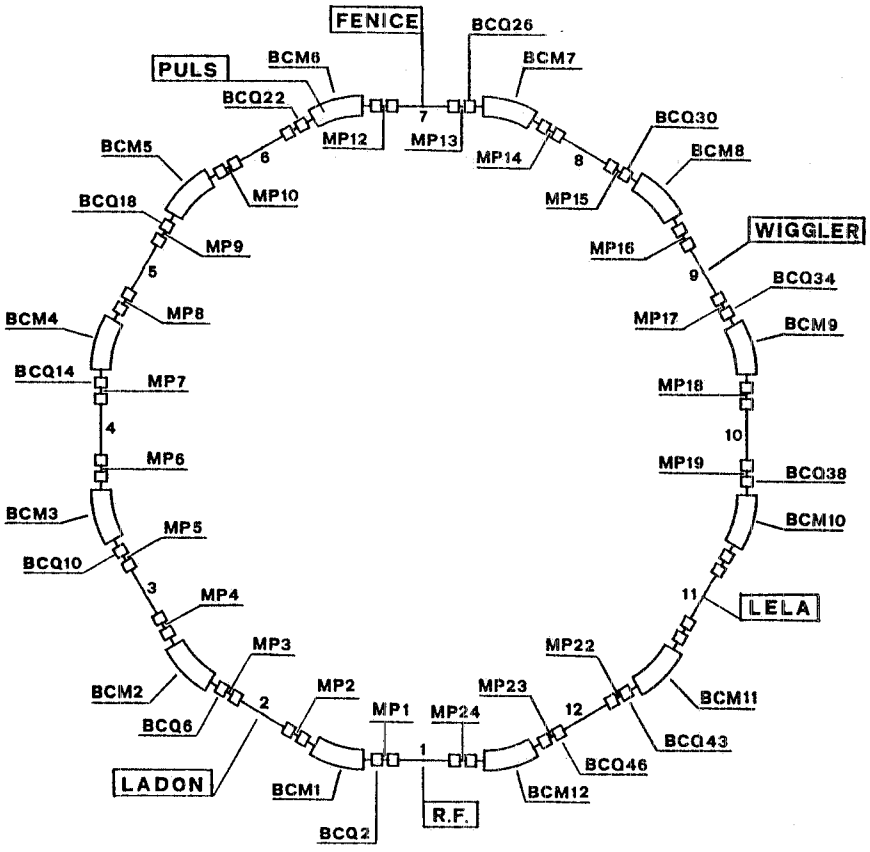

FIG. 8 - Schematic layout of the storage ring with BPM's and correctors. MP = Beam position monitor, BCQ = vertical corrector, BCM = horizontal corrector.

The correctors are calibrated with the following procedure (Ref.8):

- the betatron tunes are measured by kicking the beam with a variable frequency oscillator and observing the beam size increase on a synchrotron radiation monitor
- the theoretical displacement induced by the corrector in each BPM is calculated for a unit angular perturbation localized in the center of the corrector at the measured working point from the machine lattice model
- the angle given by a known excitation current in the corrector is found from a least squares fit of the measured points to the calculated ones.

Figg. 9 and 10 show the result of the fit for the horizontal and vertical planes. The angular deflection (δ) obtained for given correction current (I) and beam energy (E)is

$$\delta_{r,v}\,(\text{mrad}) = K_{r,v}\, I\,(A)/\, E\,(\text{Gev}) \qquad (8)$$

where $K_{r,v}$ is the calibration factor. We get for the vertical plane

$$K_v = 0.133 \pm 0.008 \quad \text{mrad.Gev/A} \qquad (9)$$

where the quoted error takes into account both experimental uncertainties and physical differences between the coils. The maximum current in the vertical correctors is 30 A.

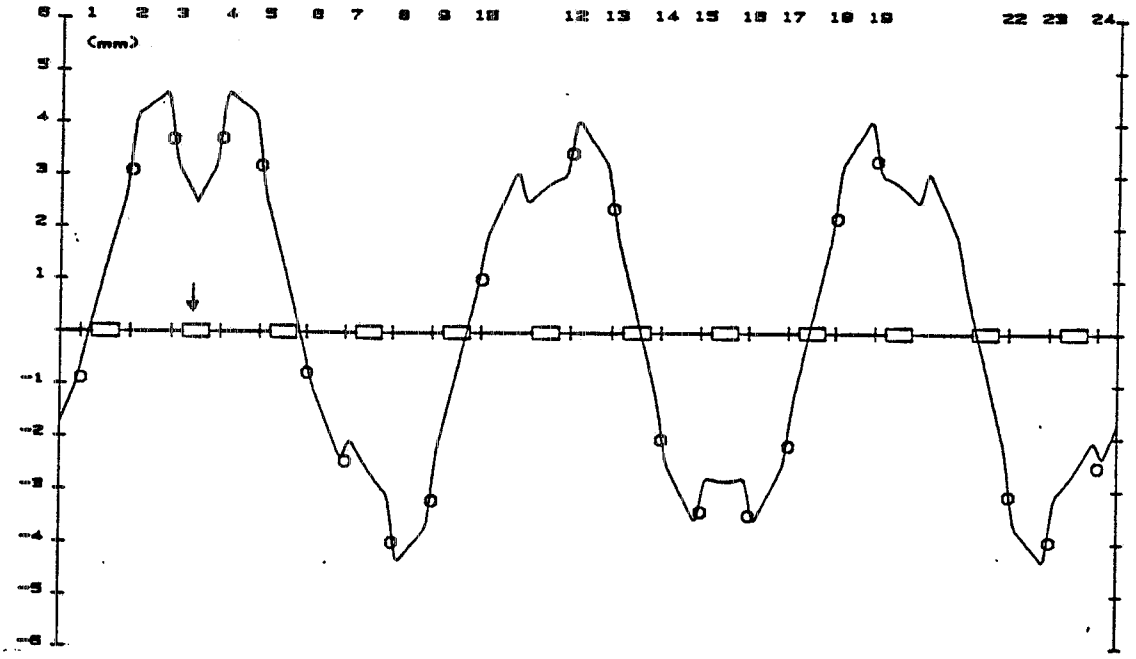

FIG. 9 - Calibration of a horizontal corrector (BCM2). The measured positions at the BPM's (dots in the figure) are obtained by subtraction of the positions with the correctors off from those with the correction on. The line through the experimental points is the beam path calculated with a theoretical lattice model with a localized angular perturbation in the second bending magnet.

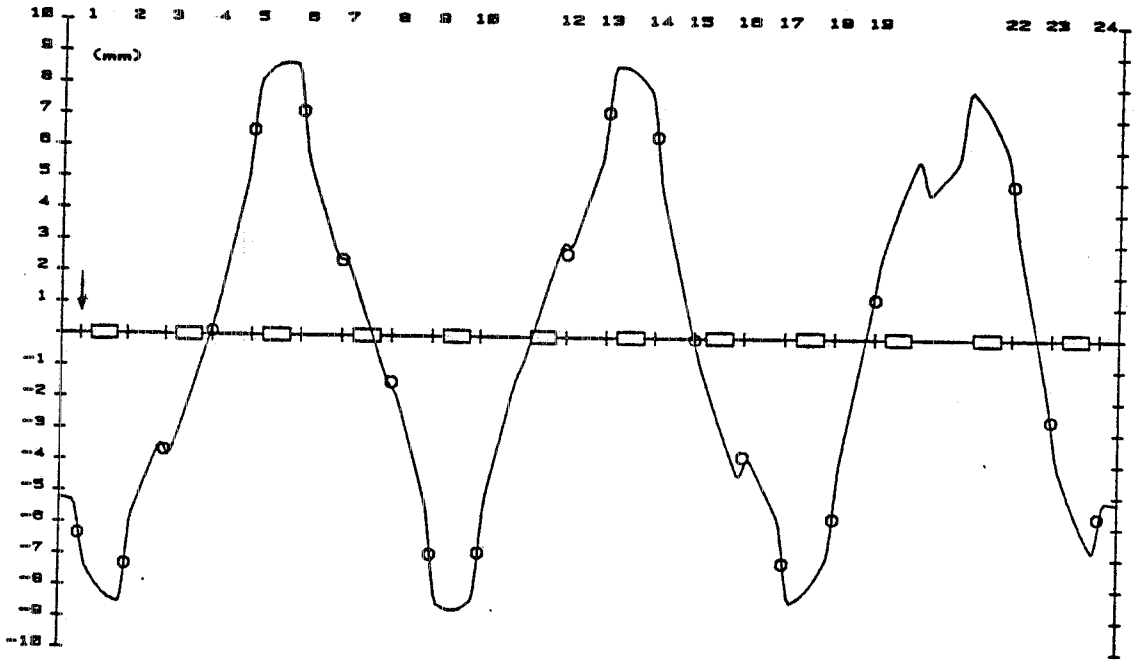

FIG. 10 - Calibration of a vertical corrector (BCQ2). The position of the angular perturbation is indicated with an arrow.

For the horizontal windings the efficiency depends slightly on the principal field in the bending magnet; the calibration factor for the horizontal correctors has been defined as

$$K_r = K_R F_r(E)$$
$$K_R = 0.587 \pm 0.018 \ \text{mrad.Gev/A} \qquad (10)$$

and the function $F_r(E)$, which exhibits a ≈30% variation throughout the energy range of the storage ring, is plotted in Fig. 11. The maximum horizontal corrector current is 1.8 A.

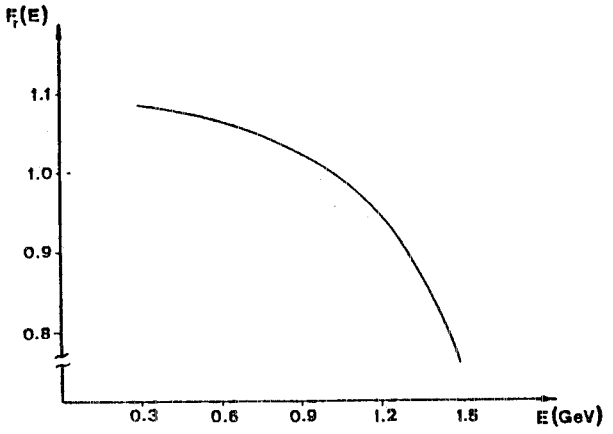

FIG. 11 - Dependence of the horizontal calibration factor on beam energy F_r (E).

5 - BETATRON TUNE MEASUREMENT

The particularly simple configuration of the storage ring lattice in its normal operation mode allows an easy measurement of the betatron tunes: focusing in both planes is provided by two symmetrical quadrupole doublets per cell (see Fig. 6), so that only two independent variables (the gradients in the quadrupole doublets) are used to adjust the betatron tunes. The choice of the working point fixes the behaviour of the β functions in the whole machine, and therefore the betatron phase of any position in the ring. β functions and phase advances in one plane are very weakly affected by the choice of the tune in the other one in the range of working points for the machine ($3.05 \leq = Q_{x,y} \leq = 3.25$). Moreover the β function at any point in the lattice does not depend much on the betatron tune in its own plane (the variation $\Delta\beta/\beta$ is of the order of $\Delta Q/Q$).

The displacement Δz_i (z=x,y) at the i-th monitor due to an angular kick δ_j in the j-th corrector, in the point-like approximation, is given by

$$\Delta z_i = \frac{(\beta_i \beta_j)^{1/2}}{2 \sin \pi Q} \cos (\pi Q - |\mu_i - \mu_j|) \delta_j \qquad z = x,y \qquad (11)$$

where β is the betatron function, Q the betatron wavenumber and μ the phase advance. If the phase advance from the corrector to the BPM is properly chosen (i.e. the cosine term in (11) is

near unity), the displacement Δz measured at the BPM is proportional to δ according to the simple relation

$$\Delta z = K_q L \delta F_q(\Delta Q)/ (\sin \pi \Delta Q) \qquad (12)$$

where K_q is a constant, ΔQ is the difference between the betatron wavenumber and the nearest integer, and $F_q(\Delta Q)$ is a correction, which takes into account the dependence of the β functions and the cosine term in (11) on the betatron tune (Ref.9). The maximum difference between $F_q(\Delta Q)$ and unity in the range of working points in the normal machine configuration is 0.05.

The behaviour of $F_q(\Delta Q)$ for the two planes can be calculated theoretically with the storage ring model, and it is shown in Fig. 12. Formula (12) can be easily inverted to give ΔQ as a function of the measured displacement at the chosen BPM and of the current in the chosen correctors, using the calibration factors (9) and (10).

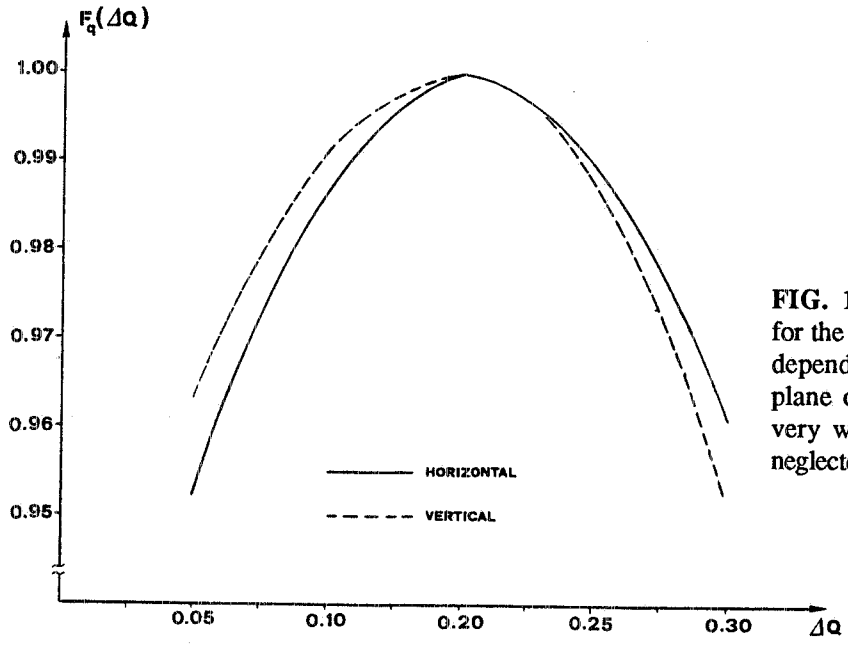

FIG. 12 - Correction factor $F_q(\Delta Q)$ for the betatron tune measurement. The dependence of the correction in one plane on the tune in the other one is very weak, and it has therefore been neglected.

It should be pointed out that the measurement of the betatron tunes by this method is not an absolute one, since it relies on the corrector calibration obtained with the tune measurement with the variable frequency oscillator. However, once the calibration factors have been measured, it is much easier to measure the tunes with the method described here. The complete procedure of corrector excitation in a horizontal (BCM3) and a vertical (BCQ10) corrector, beam position measurement at a pick-up station (BPM6) and tune calculation through (12) has been implemented on the storage ring control computer.

The betatron tune values measured with the above described method agree with those measured with the variable frequency oscillator within $\Delta Q/Q \approx 3 \times 10^{-3}$.

6 - CLOSED ORBIT CORRECTION

Several strategies for closed orbit correction have been studied and applied in accelerators and storage rings. We chose the Least Squares method (Ref.10), which proves to be easier to use, particularly when different lattice configurations and working points are foreseen in the ring operation (see Par.4).

This Least Squares method attempts to minimize the rms displacement at the monitor positions. The overall effect of the correctors on the closed orbit can be expressed in matrix notation as

$$\overrightarrow{\Delta Z} = T \vec{\delta} \tag{13}$$

where T is an NxM matrix (N and M are the numbers of monitors and correctors respectively) whose elements are

$$T_{ij} = \frac{(\beta_i \beta_j)^{1/2}}{2 \sin \pi Q} \cos (\pi Q - |\mu_i - \mu_j|) \tag{14}$$

The values of the angular kicks δ_j are determined by the requirement that the sum

$$S = \sum_1^N{}_i (\Delta z_i + z_i^\circ)^2 + K \sum_1^M{}_j \delta_j^2 \tag{15}$$

be a minimum. z_i° are the measured positions of the beam at the BPM's before the correction. The factor K (Ref.11) has been introduced to allow for a reduction in required corrector strengths, if the maximum currents are exceeded: obviously, the residual closed orbit after correction will be in this case larger than that obtained for K = 0.

The condition for S to be a minimum is

$$\sum_1^N{}_i (\Delta z_i + z_i^\circ) T_{ij} + K \delta_j = 0 \qquad j = 1, 2, \ldots, M \tag{16}$$

or, in matrix notation

$$T^T (\overrightarrow{\Delta Z} + \vec{Z}^\circ) + K I \vec{\delta} = 0 \tag{17}$$

where T^T denotes the transpose of T and I is the unitary matrix. Inserting (13) into (17) we get

$$T^T \vec{Z}^\circ + (T^T T + K I) \vec{\delta} = 0 \tag{18}$$

and then, if the number of monitors in not smaller than the number of correctors, the solution can be obtained from

$$\vec{\delta} = -(T^T T + K\, I)^{-1}\, T^T \vec{Z^\circ} \qquad (19)$$

This method requires a MxM matrix inversion: for this purpose we use the CERN library routine MATIN2, which is sufficiently accurate (in our case M≤12).

A computer program has been implemented on the storage ring control computer (Ref.12) to perform the whole procedure of orbit correction. Since this is needed in many different operating conditions, the procedure has been written as a sequence of steps, some of which can be skipped by the operator if not required. These are indicated with an S in the following flowchart:

a (S) - set of all correctors to zero excitation and cycle of all the magnet backleg windings

b (S) - measurement of betatron tunes

c - calculation of matrix elements T_{ij} at the measured (or known) working point with the storage ring lattice model

d - measurement of the closed orbit

e(S) - calculation of the angular kicks (19) and check of the required corrector currents. If the maximum range is exceeded, the operator is asked to enter a larger value for K (see (15)). The foreseen residual orbit is displayed. The calculation is performed separately for the horizontal and vertical planes, so that the correction can be made in a single plane only

f(S) - Set of the required corrector currents, separately for the two planes

g - measurement of the corrected closed orbit.

Figg.13 e 14 show the result of the closed orbit correction procedure at a beam energy of 0.95 Gev, with betatron tunes $Q_x = 3.18$, $Q_z = 3.23$. In the horizontal plane (Fig. 13) the closed orbit due to magnetic elements misalignment is ≈±5 mm, while the residual orbit after correction is ≈±0.8 mm. In the vertical plane (Fig. 14) the closed orbit is reduced from ≈±3 mm to ≈±0.3 mm.

In the horizontal plane the residual closed orbit lies well within the typical transverse beam size; this is true also for the vertical plane if the beam is in full coupling.

The Least Squares method tends to compensate monitor position errors: the compensation can in principle be total if the number of correctors is equal to the number of monitors. In our case the number of correctors is approximately half of the number of monitors, so that the method can compensate only a fraction of monitor positioning errors. Since the positioning accuracy has been estimated to be of the order of 0.2 mm, the overall orbit correction accuracy (with respect to the quadrupole axes) comes out to be better than ±1.0 mm in the horizontal plane, and better than ±0.5 mm in the vertical one.

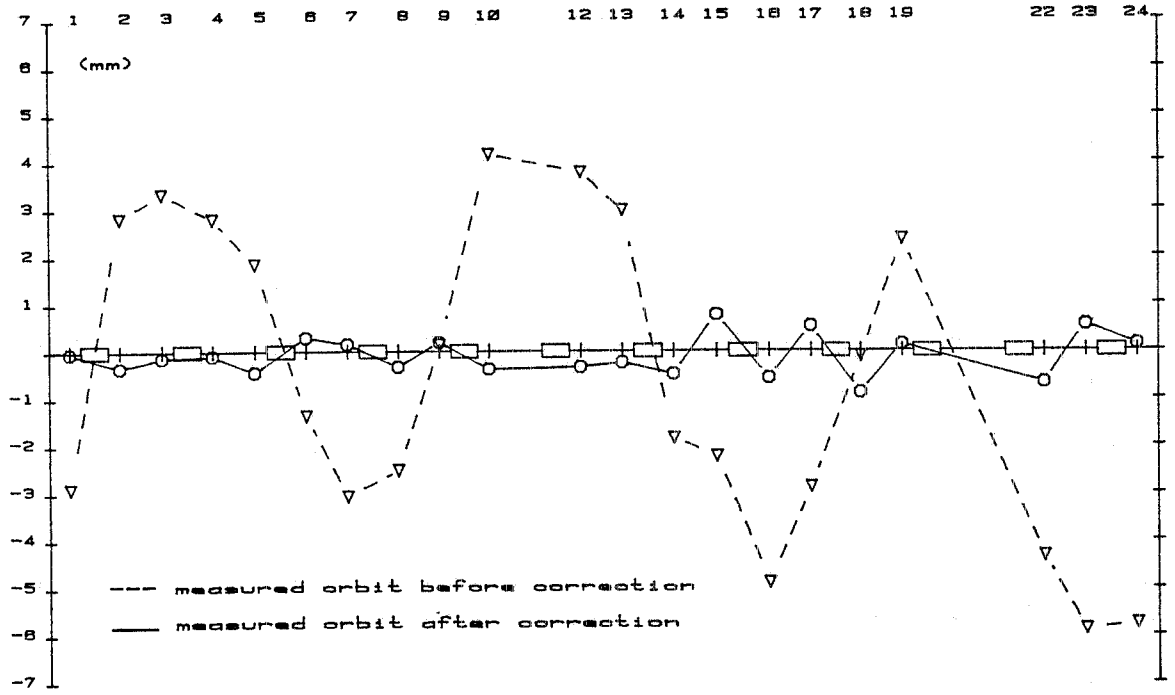

FIG. 13 - Horizontal closed orbit correction. The energy is 0.95 Gev, betatron tunes Q_X=3.18, Q_Z=3.23.

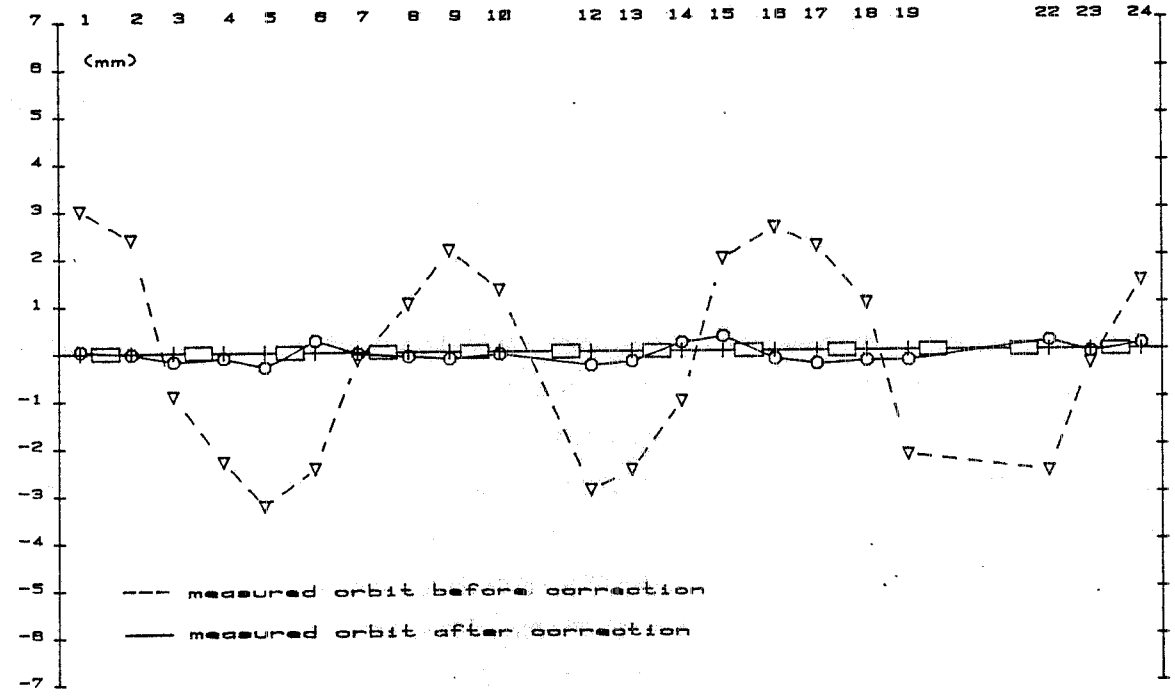

FIG. 14 - Vertical closed orbit correction. The energy is 0.95 Gev, betatron tunes Q_X=3.18, Q_Z=3.23.

7 - LOCALIZED ORBIT BUMPS

Beam steering is often required to optimize the performance of an experimental beam line. In Adone up to 3 source points can be used at the same time for synchrotron radiation and nuclear physics experiments, and therefore it can be useful to change beam position and angle in both planes at a given source point, while leaving the closed orbit unchanged elsewhere. This procedure is also called an "orbit bump".

The most general steering of the beam at a given point P requires 4 correctors in each plane (see Fig. 15). If the beam must be moved by a displacement Z_p and an angle Z'_p with respect to the initial orbit, the angular kicks δ_1 and δ_2 in the 2 upstream correctors are obtained by solving the linear system (Ref.13)

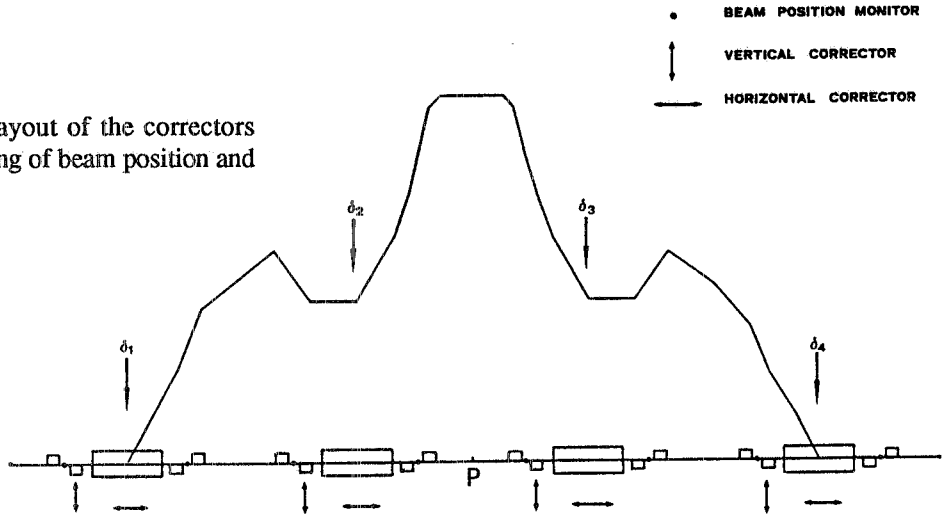

FIG. 15 - Schematic layout of the correctors used for localized steering of beam position and angle at a source point.

$$Z_p = (\beta_p)^{1/2} \sum_{1}^{2}{}_j \delta_j (\beta_j)^{1/2} \sin \Delta\mu_{jp}$$

$$Z'_p = (\beta_p)^{-1/2} \sum_{1}^{2}{}_j \delta_j (\beta_j)^{1/2} (\cos \Delta\mu_{jp} - \alpha_p \sin \Delta\mu_{jp}) \qquad (20)$$

where α_j and β_j are the Twiss functions at the corrector positions α_p is calculated at point P and $\Delta\mu_{jp}$ are the betatron phase advances from the correctors to point P. In order to have no change in beam position before the first and after the last corrector used for the orbit bump, the downstream angular kicks δ_3 and δ_4 must be

$$\delta_3 = - [\sum_{1}^{2}{}_j \delta_j (\beta_j)^{1/2} \sin \Delta\mu_{j4}] / [(\beta_3)^{1/2} \sin \Delta\mu_{34}]$$

$$\delta_4 = - (\beta_4)^{-1/2} \sum_{1}^{3}{}_j \delta_j (\beta_j)^{1/2} (\cos \Delta\mu_{j4} - \alpha_4 \sin \Delta\mu_{j4}) \qquad (21)$$

Fig. 16 shows an orbit bump of 10 mm in the vertical plane with no angle in the center of

straight section n.3. The experimental points are measured at the BPM's by subtracting the position measurements without the orbit bump from those with it: in this representation zero displacement means that the beam position at the BPM's outside the bump does not change when this is switched on. The line through the experimental points is the beam path calculated with the theoretical model with localized angular kicks at the center of the correctors. It can be seen from Fig. 16 that the beam position variation outside the bump is less than 0.2 mm.

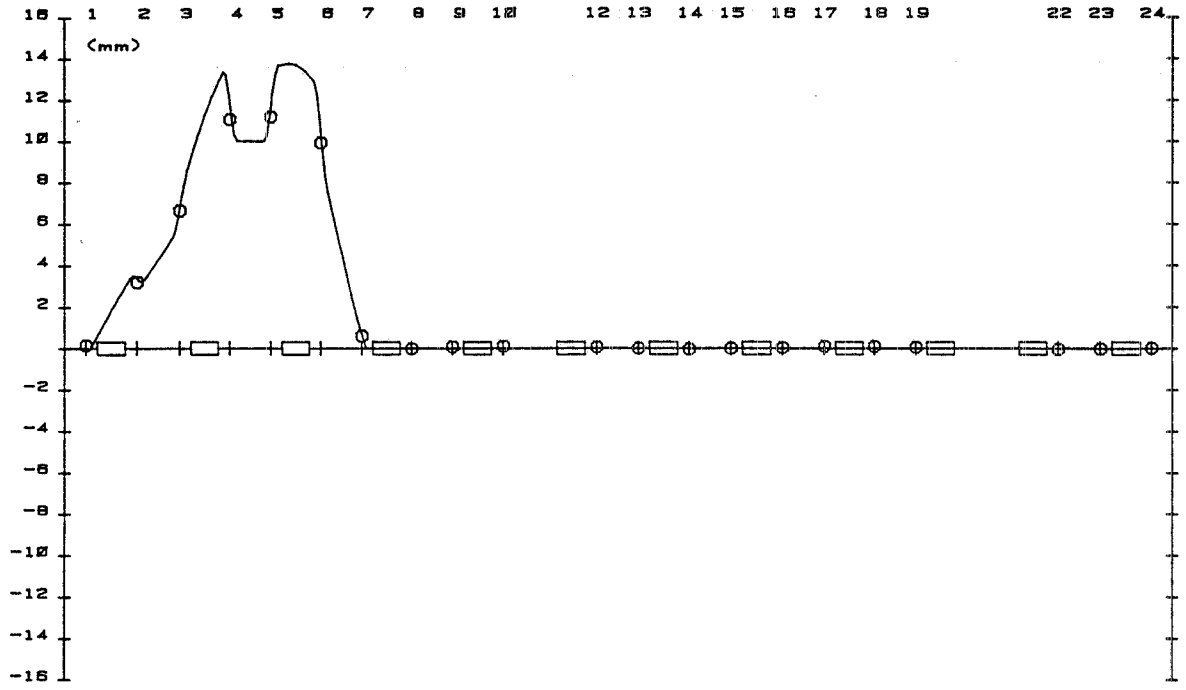

FIG. 16 - Vertical orbit bump in straight section n.3 (Y_p = 10 mm, Y'_p = 0). The measured points are obtained by subtracting the positions without the orbit bump from those measured with the bump on. The line through the dots is the calculated beam path with the lattice model with localized angular perturbations in the center of the quadrupoles.

The increase in orbit length created by orbit bumps in the vertical plane is a second order effect, which can be neglected in all practical cases. This is not true for the horizontal plane, where any orbit distortion gives a net path difference in the bending magnets. It can be shown that, in the absence of any constraint on the total orbit length, a set of N horizontal angular kicks δ_j at points where the dispersion function is ψ_j creates a relative orbit lengthening

$$\Delta L/L = (1/L) \sum_{1}^{N}{}_j \psi_j \delta_j \qquad (22)$$

In electron storage rings, however, the total orbit length is constrained by the synchronism condition with the RF frequency: the energy of the beam is forced to change in order to compensate the orbit lengthening (22) and the relative energy change is

$$\Delta E/E = - (1/\alpha_c)\ \Delta L/L \qquad (23)$$

where α_c is the momentum compaction factor. The effect is of the order of 10^{-4} for a single angular kick of 1 mrad in the bending magnet, and it shows up in the BPM's outside the bump as a displacement

$$\Delta X = \psi_{bpm}\, \Delta E/E \qquad (24)$$

where ψ_{bpm} is the dispersion function at the BPM's. Fig. 17 clearly shows this phenomenon, which can of course be compensated by changing the RF frequency by $\Delta f/f = - \Delta L/L$. The second series of beam positions in Fig. 17 has been measured after changing the RF frequency : the points are all at the same distance from those measured before this correction, because the dispersion function has the same value in all BPM's.

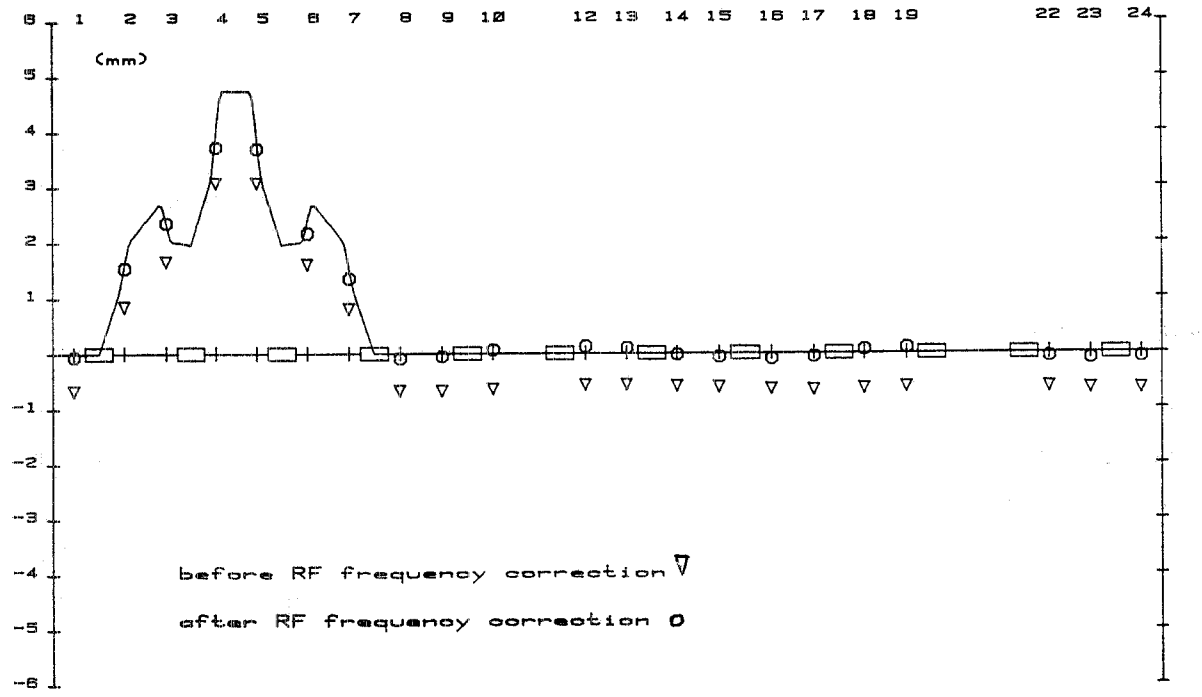

FIG. 17 - Horizontal orbit bump in the center of straight section n.3 (X_p = 5 mm, X'_p = 0). before and after correction of the energy shift with the RF frequency. The angular kicks required for this bump are symmetric with respect to the source point.

Fig. 18 shows an horizontal orbit bump requiring an angle of 0.5 mrad in straight section n.3 with no displacement: in this case the position of the beam outside the bump is not displaced because the kicks are antisymmetric with respect to the center of the straight section, so that the sum in (24) vanishes.

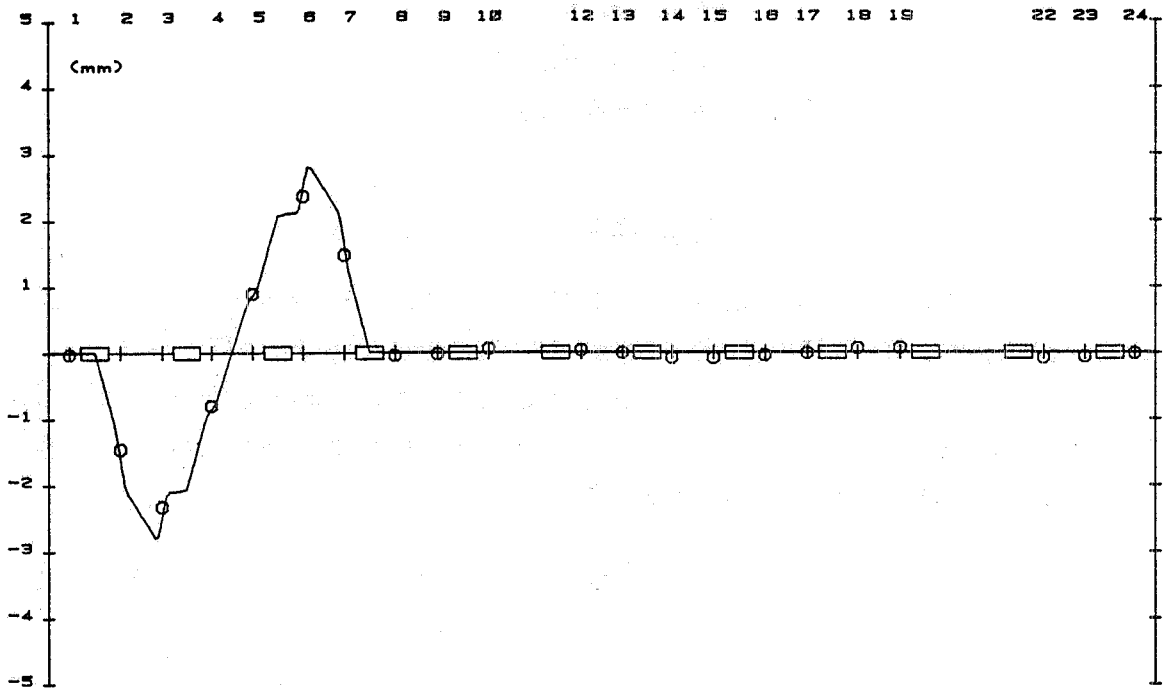

FIG. 18 - Horizontal orbit bump in the center of straight section n.3 ($X_p = 0$, $X'_p = 0.5$ mrad). The angular kicks required for the bump are antisymmetric with respect to the source point.

8 - CONCLUSIONS

The system went into operation smoothly and in a predictable way. Its precision and reproducibility are excellent and it is used routinely as a reliable diagnostic and operational tool. Closed orbit correction can be performed with the accuracy required for the operation of synchrotron radiation, nuclear physics and free electron laser experiments. Beam steering by means of localized orbit bumps proved to be very useful to improve injection and compatibility between different experiments.

ACKNOWLEDGEMENTS

The results presented in this paper are due to the effort and thorough work af most members of the Machine staff. We thank them all.

We are particularly indebted to M. Bassetti for many clarifying discussions, to V. Chimenti for constant advice during the BPM project and assembly, to C. Marchetti for the realization of the electronic equipment and to G. Serafini for the mechanical support.

A. Vitali designed the calibration bench. We all remember him.

We wish to thank also J.Borer and G.Vismara (CERN) for helpful discussions about the button design and the position algorithm.

REFERENCES

(1) J.H. Cupérus - "Monitoring of particle beams at high frequencies" - NIM Vol.145 (1977) pp. 219-231.
(2) J. Borer, C. Bovet - "Computed response of four pick-up buttons in an elliptical vacuum chamber" - LEP note 461 (1983).
(3) S. De Simone, S. Fortebracci, M. Serio - "Amplificatori accordati" - Adone Internal Memorandum SC-126 (1986).
(4) S. De Simone, M. Serio - "Multiplexer per monitor di posizione" - Adone Internal Memorandum SC-121 (1985).
(5) M. Preger - "Misura del campo magnetico generato dalle bobine di correzione nei magneti di Adone" - Adone Internal Memorandum SC-128 (1986).
(6) M. Serio, A. Aragona, V. Lollo, G. Serafini - "Adone 1986 - Strumentazione e camera da vuoto" - Adone Internal Memorandum SC-120.
(7) R. Barbini, G. Vignola, S. Trillo, R. Boni, S. De Simone, S. Faini, S. Guiducci, M. Preger, M. Serio, B. Spataro, S. Tazzari, F. Tazzioli, M. Vescovi, A. Cattoni, C. Sanelli, M. Castellano, N. Cavallo, F. Cevenini, M. Masullo, P. Patteri, R. Rinzivillo, A. Cutolo, S. Solimeno - "Preliminary results of the Adone storage ring FEL experiment, LELA" - Proceedings of the Bendor Free electron laser Conference, Bendor (France), 1982 M. Biagini, R. Boni, S. De Simone, S. Guiducci, M. Preger, M. Serio, S. Tazzari, F. Tazzioli, M. Vescovi, M. Ambrosio, G. Barbarino, M. Castellano, N. Cavallo, F. Cevenini, M. Masullo, P. Patteri, R. Rinzivillo, S. Solimeno, A. Cutolo - "Gain of the LELA free electron laser and characteristics of the optical cavity" - Proceedings of the 1984 Free Electron Laser Conference, Castelgandolfo (Italy) 1984.
(8) S. De Simone, E. Gianfelice, S. Guiducci, S. Pella, M. Preger, M. Serio - "Correzione dell'orbita di errore in Adone" - Adone Internal Memorandum RM-31 (1986).
(9) M. Preger - "Misura delle frequenze di betatrone con i monitors a bottone" - Adone Internal Memorandum SC-127 (1986).
(10) A.S. King, M.J. Lee, P.L. Morton - "Closed orbit correction in SPEAR" -SLAC-PUB-1203 (A) (1973).
(11) E. Gianfelice - "Programma per la correzione on-line dell'orbita chiusa di Adone" - Adone Internal Memorandum SC-125 (1987).
(12) E. Gianfelice, S. Pella, M. Preger - "Programma per la correzione automatica dell'orbita di errore in Adone" - Adone Internal Memorandum SC-129 (1987).
(13) C. Biscari, M. Preger - "Bumps localizzati in Adone" - Adone Internal Memorandum SC-130 (1987).